Document Change Log

Revision	Date	Affected Portions and Description
	10 May 2018	Original release

Which Product Versions Does this Document Cover?

Product Filename Prefix	Version Number in Filename	Brief Description
AirMSPI_ER2_GRP_ELLIPSOID	V006	L1B2 Ellipsoid-Projected Georectified Radiance and Polarization Data
AirMSPI_ER2_GRP_TERRAIN	V006	L1B2 Terrain-Projected Georectified Radiance and Polarization Data

TABLE OF CONTENTS

1 INTRODUCTION

The purpose of this document is to describe the data quality of the AirMSPI L1B2 products specifically for the Radar Definition Experiment (RADEX) field campaign, which was based out of Joint Base Lewis-McChord (JBLM), WA, and included flights over California, Washington, and the Pacific Ocean. AirMSPI imagery was acquired from 10 November to 13 December 2015.

1.1 AirMSPI L1B2 Products

The Airborne Multiangle SpectroPolarimetric Imager (AirMSPI) Level 1B2 products contain radiometric and polarimetric observations of clouds, aerosols, and the surface of the Earth made from the National Aeronautics and Space Administration's (NASA) ER-2 high altitude research aircraft. The AirMSPI instrument acquires data using one of two possible modes, step-and-stare and sweep. Step-and-stare data are gridded with 10 m spatial sampling, with one file provided for each view angle. Sweep data are gridded with 25 m spatial sampling. Files are distributed in HDF-EOS-5 format.

The instrument reports for eight spectral bands (355, 380, 445, 470, 555, 660, 865, and 935 nm) the incident radiance (Stokes *I)*, complemented with the linear polarization state (Stokes *Q* and *U*) in three of the bands (470, 660, and 865 nm) for a total of 14 channels.

1.2 AirMSPI Data Processing and Distribution

The MISR Science Computing Facility (SCF) at the Jet Propulsion Laboratory (JPL) supports the development of AirMSPI science algorithms and software, instrument calibration and performance assessment, and also provides quality assessment and data validation services with respect to AirMSPI Science Data Processing (SDP). The MISR SCF is used to perform the standard processing of the AirMSPI data. After AirMSPI data processing is complete, the standard output products are archived and made available to users via the Langley Research Center (LaRC) Atmospheric Science Data Center (ASDC) client services. See https://eosweb.larc.nasa.gov/project/airmspi/airmspi_table.

1.3 Controlling Documents

1) Multiangle Spectropolarimetric Imager (MSPI) Algorithm Theoretical Basis Document Rev. B Draft, November 2009 (or latest version).

1.4 Related Documents

1) AirMSPI Data Product Specification for the AirMSPI Level 1B2 Products (V006), JPL D-100825, Rev. C, September 2017 (or latest version).

2 RADIOMETRIC CALIBRATION

2.1 Laboratory Calibration

Laboratory radiometric calibration of the AirMSPI instrument (Diner et al., 2013a) was conducted on 30 March 2016 (after the RADEX and SPEX-PR field campaigns) by observing the output port of a 1.65 m integrating sphere. The sphere illuminates the entire field of view of the instrument. Data were collected at multiple light levels and the sphere output was monitored with an Analytical Spectral Devices (ASD) FieldSpec Pro spectrometer in order to generate a digital number (DN) vs. radiance regression for each pixel. The AirMSPI line arrays have 1536 pixels in each channel. Offset levels are determined from observations in 100 pixels at the end of each array that are shielded from illumination; hence only 1436 pixels in each line collect image data. After correction for non-linearity (lincal), gain factors are computed on a per-pixel basis for each channel. The 13 spectral channels of the instrument measure incident radiance at wavelengths close to 355, 380, 445, 470, 555, 660, 865, and 935 nm (8 bands). In keeping with Stokes parameter nomenclature, the polarization channels report I, Q, and U, where I is the total measured radiance. The Stokes parameters Q (excess of horizontally over vertically polarized light) and U (excess of 45° over 135° polarized light) are reported for the bands at 470, 660, and 865 nm. Note that the AirMSPI instrument does not have a separate radiance-only channel at 470 nm. The radiance reported in the AirMSPI data products for this channel is obtained independently from the demodulated 470Q and 470U channel data and is the mean of the values derived from these two channels. Thus, although the AirMSPI instrument itself only has 13 spectral channels, 14 spectral channels are reported in the AirMSPI L1B2 products.

Although gain factors are derived on a per-pixel basis, residual striping can appear in Earth images, particularly in the UV bands. It is believed that this striping is the result of out-of-band spectral leakage due to physical imperfections in the focal plane filter.

2.2 Vicarious Calibration

On 10 November 2015, AirMSPI overflew the parking lot at Hangar 703, Armstrong Research Flight Center. Data were taken both from the air, and by a team on the ground. For the latter, both the reflectance of the parking lot, surface pressure, and aerosol loading measurements were made. Instrumentation included an Analytic Spectral Devices (ASD) field spectrometer and a Microtops sunphotometer. These data were used as input to the Markov radiative transfer code, which produced top-of-atmosphere spectral radiances. The Markov code is a vector code, tracing polarization components through the atmosphere. This vicarious calibration of AirMSPI had band-dependent agreement with the laboratory calibration. Differences ranged from 15% in the UV to 1% agreement in the mid-visible. The radiometric calibration of AirMSPI was set using this vicarious calibration. It is believed to have a higher accuracy than the laboratory calibration, due to the low UV light levels used to calibrate in the laboratory.

2.3 Calibration Traceability

AirMSPI calibrations are traceable to *Système international* (SI) Units, via National Institute of Standards and Technology (NIST) standards. For laboratory calibrations, this is through a reference 20.32 cm (8 inch) integrating sphere, calibrated annually by the vendor, Gooch & Housego (http://goochandhousego.com/). For vicarious calibrations, this is through a Spectralon reflectance standard located at the vicarious calibration site.

2.4 Radiometric Data Quality Indicators

Following the practice adopted by the Multi-angle Imaging SpectroRadiometer (MISR) project, each AirMSPI pixel is assigned a Radiometric Data Quality Indicator (RDQI). The RDQI definitions are as follows:

RDQI = 0: No radiometric issues are identified.

RDQI = 1: The radiometric quality does not meet an identified threshold but is deemed usable for scientific analysis purposes.

RDQI = 2: The radiometric quality does not meet a secondary threshold and the data from this pixel should not be used for scientific analysis purposes.

RDQI = 3: The quality of the pixel is scientifically and cosmetically unusable. In addition, the shielded pixels at the end of each line array are marked with RDQI of 3.

During laboratory calibration, a "gain" is computed from the slope of camera output DN to total-band incident radiance, *I*. It is observed that pixels with a large out-of-band leakage have a larger uncertainty in this gain, in that it is observed to vary with the spectrum of the incident light. A data quality indicator can thus be computed based on the change in gain with different illumination sources. Specifically, we take the ratio of the gain computed with an incandescent lamp to the gain computed from adding a UV plasma lamp. Pixels for which this gain ratio is between 0.95 and 1.05 are assigned an RDQI value of 0 indicating that out-of-band light is a small contributor to the measured radiance. Pixels for which the gain ratio is outside of this range, but between 0.90 and 1.10 are assigned an RDQI value of 1. Pixels with gain ratios outside both these ranges, but between 0.80 and 1.20 are assigned an RDQI value of 2. All other pixels are assigned an RDQI value of 3. Note that for the 470I channel, for which the reported radiance is the mean of the demodulated 470Q and 470U channel data, the RDQI is likewise calculated as the mean (rounded to the nearest integer) of the RDQI values for these two channels. The observed out-of-band leakage is believed to be the cause of striping in the images, which is particularly noticeable in the UV bands.

As described above, for the 470 nm radiance channel, information from two polarimetric channels – a channel measuring *I* and *Q*, and a channel measuring *I* and *U* – is used to generate the data reported in the L1B2 product. The RDQI values reported for the 470 nm *I* radiance channel represent the maximum of the values reported separately for these two channels. For the 660 and 865 nm bands, three channels are used to generate the data reported in the L1B2 product: a channel

measuring *I* only, a channel measuring *I* and *Q*, and a channel measuring *I* and *U*. The RDQI values reported for these channels represent the values in the non-polarimetric *I* channel, and are typically 0.

Pixels marked with RDQI = 0 are expected to have an absolute radiometric uncertainty of ~5% (1σ). This radiometric uncertainty is attributed to the vicarious calibration methodology, which sets the absolute radiometric scale. The laboratory calibration is used to establish the relative-pixel response, also known as "flat-fielding".

3 SPECTRAL CALIBRATION

Determination of the detailed spectral response function (SRF) of each AirMSPI channel has been made based on the laboratory calibration of 9 December 2013. A monochromator was used for this purpose. The SRF is equal to the camera response to monochromatic light normalized by a silicon diode response. The monochromator provided wavelength scans from 300 to 2500 nm. Two sources were used in separate spectral scans of all channels — a Luxim Light Emitting Plasma lamp for ultraviolet-blue, and a quartz-halogen lamp for the remaining visible and near-infrared channels. The results of this calibration are shown in Table 1 and Figure 2.

In the current product release (V006), center wavelengths, effective (equivalent square-band) bandwidths, and effective (equivalent square-band) transmittances are calculated by applying the moments method of Palmer (1984) to the normalized spectral response of each band over the range 300-1100 nm. Solar irradiances are weighted by the total-band spectral response. The Wehrli (1985) extraterrestrial solar spectrum was used for this purpose. These values are provided in Table 1 below, and represent the total-band response. Again, the values reported for the 470I channel represent the mean of the demodulated 470Q and 470U channel values.

In general, radiometric response at wavelengths far from the "in-band" spectral region is estimated at $< 10^{-4}$ of the peak response, though as noted above, a larger amount of out-of-band leakage is present in a small subset of pixels in the UV bands, leading to striping in a portion of the UV images. Currently uncorrected striping in the 355 and 380 nm bands is attributed to filter blemishes that create a scene-dependent scattered light response.

Table 1 – Total-band effective center wavelength, bandwidth and transmittance, and total-band weighted solar irradiance E_0 [W m^{-2} nm^{-1}] at 1 AU

Channel Name	Center Wavelength (nm)	Effective Bandwidth (nm)	Effective Transmittance	Solar Irradiance (W m^{-2} nm^{-1})
355I	355.1	47.7	0.609	1.002
380I	377.2	40.4	0.750	1.079
445I	443.3	46.0	0.799	1.861
470I	469.1	45.5	0.824	2.000
470Q	469.4	45.0	0.837	1.999
470U	468.8	46.0	0.815	2.000
555I	553.5	38.6	0.758	1.857
660I	659.2	45.2	0.835	1.555
660Q	659.1	43.8	0.881	1.556
660U	659.1	48.2	0.798	1.556
865I	863.3	43.5	0.829	0.976
865Q	863.7	45.6	0.810	0.976
865U	864.1	48.5	0.753	0.975
935I	931.3	53.2	0.809	0.823

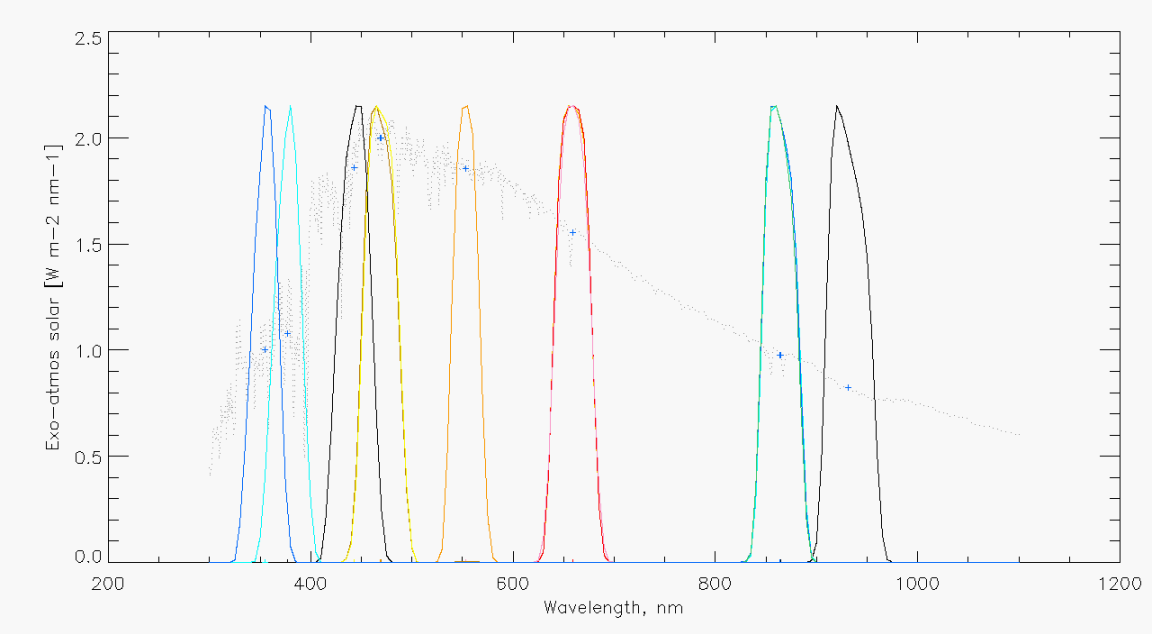

Figure 2. AirMSPI spectral response functions (SRF) shown in colored lines with the Wehrli (1985) exoatmospheric solar irradiance values shown in the faint, gray, dotted line. E0 values at 1 AU are indicated by the "+" symbol.

4 POLARIMETRIC CALIBRATION

AirMSPI uses a time-varying retardance in the optical path to modulate the orientation of the linearly polarized component of the incoming light, described by the Stokes components Q (excess of horizontally over vertically polarized light) and U (excess of 45º over 135º polarized light) (Diner et al., 2007, 2010; Mahler et al., 2011). As a result, the ratios of these parameters to the radiance I, given by $q = Q/I$ and $u = U/I$ are to first order insensitive to the absolute radiometric calibration of a given pixel because both the numerator and denominator are determined from signals acquired by the same detector element. The degree of linear polarization (DOLP) and angle of linear polarization (AOLP) derived from these ratios, equal to $\sqrt{q^2 + u^2}$ and $0.5\tan^{-1}(u/q)$, respectively, are likewise insensitive to absolute radiometric calibration, based on similar considerations. To compensate for instrumental polarization aberrations (e.g., mirror diattenuation, imperfect retardance), a set of 10 polarimetric calibration coefficients is established for every pixel (Diner et al., 2010; Van Harten et al., 2018).

Two specialized pieces of equipment exist for verifying and controlling the performance of the polarimetric measurement approach during in-flight operations of AirMSPI. The first is an optical probe, which continuously sends a beam of light through the photoelastic modulators (PEMs) to monitor their retardances and phases. The information from the probe shows how far the PEM retardances and phases are from their desired values. A feedback control system within the instrument then adjusts the PEM parameters to drive the error signals to zero. Test data demonstrated the ability to control the PEM retardance and phase parameters to within a fraction of 1 mrad, keeping contributions to the overall DOLP uncertainty budget at <0.001. The second polarization monitoring system is an external polarization validator, which consists of nine light-emitting diodes (LEDs), three each at the AirMSPI polarimetric bands, that illuminate a plastic diffuser. In front of the diffuser, sheet polarizers are placed in different orientations. The validator is viewed before and after every multiangle observation of an Earth scene. Information from the validator system is used to derive instrument dark current and evaluate the stability of the DOLP measurements.

Results from a ground-based version of the instrument, GroundMSPI (Diner et al., 2012), show systematic DOLP uncertainties (excluding the effects of random noise), determined as the root-mean-square residual in DOLP as a polarizer is rotated in front of the camera, of ±0.003 or better. More recent results for AirMSPI, using a rotating polarizer as well as partially polarized reference samples, show systematic calibration uncertainties of ±0.001 (Van Harten et al., 2018).

5 GEORECTIFICATION AND CO-REGISTRATION

As a part of the ground data processing, AirMSPI data from all spectral bands and all viewing angles are georectified and co-registered to a common Earth-based, Universal Transverse Mercator (UTM) projection grid. Distortions that can be associated with AirMSPI's type of pushbroom remote sensing imaging are taken into account by properly defining instantaneous pixel projection rays using ancillary data such as estimates of camera internal viewing geometry and ER-2 navigation data, which provide dynamic measures of the platform altitude and attitude variations. There are two types of AirMSPI georectified data products: 1) terrain projected and 2) ellipsoid projected. Terrain-projected data use a digital elevation model (DEM) for the projection surface

so that cloud-free imagery is truly orthorectified with reference to that surface. Ellipsoid-projected data use the World Geodetic System 1984 (WGS84) Earth reference ellipsoid for the projection surface. One purpose of the ellipsoid projection is to provide input to stereoscopic height retrievals for predominantly cloudy imagery. Automatic stereoscopic retrieval software is currently in development.

Factors affecting geospatial accuracy of AirMSPI products include: 1) relative band-to-band co-registration within a single viewing angle, 2) multi-angle co-registration, and 3) absolute georectification. The uncertainty depends on the magnitude of the errors in the supplied ancillary data and errors in the projection surface defined by the DEM. In the case of the RADEX campaign, the United States Geological Survey (USGS)-provided National Elevation Dataset (NED) with 10 m horizontal posting and 2.44 m rms error in elevation is used. Errors in the ancillary data defining viewing geometry are handled as static and dynamic pointing errors in order to characterize them using available ground control points (GCPs) in a procedure based on simultaneous bundle adjustment (Jovanovic et al., 2012). For targets where there is an optimum number of GCPs available, both static and dynamic pointing errors are recovered simultaneously prior to georectification and co-registration. These data are denoted as having full geometric calibration "directly" applied with expected co-registration and georectification uncertainty of around 15 m rms across all viewing angles and all bands. For other targets, (i.e., those without available GCPs, which are mostly fully ocean or cloudy imagery), an estimate of static pointing errors made on separate flight lines within the same campaign is utilized. These products are denoted as having geometric calibration "indirectly" applied with a current estimate of georectification and co-registration uncertainty of less than one hundred meters. The type of geometric calibration is recorded in the file metadata list under the field name "Geolocation stage". Analysis and implementation efforts are still in progress with an objective to fully optimize the camera viewing model so that uncertainties of indirectly calibrated data are minimized.

Band-to-band relative co-registration uncertainty within the same viewing angle is well within 10 m, which is the pixel size of the map projection grid in the step-and-stare terrain-projected data. In the case of ellipsoid-projected data there will be some offsets in the relative band-to-band registration due to the parallax caused by the true height of the viewing surface and physical band separation in the focal plane. Additionally, slight errors in registration can cause a slight displacement (on the order of a degree or two) of polarimetric features such as the backscatter glory from their expected location.

Occasional gaps of isolated lines in AirMSPI pushbroom imagery are present in an extremely small number of scenes. These are due to changes in the ER-2 pitch attitude that occurred too abruptly (e.g., as the result of turbulence) to either: 1) be captured accurately in the ER-2 navigation data, and/or 2) cause gaps in the imagery created in the pushbroom fashion.

6 INCIDENTAL DATA QUALITY ISSUES

Occasionally, scene elements (e.g., deep clouds or sunglint) are so bright as to cause saturation in some pixels. Future versions of the AirMSPI product may flag these situations, but this has not been done for the current version of the publicly available data. Isolated pixels that experienced saturation in one or more channels are readily identifiable in the imagery due to their anomalous appearance. The following images contain saturated pixels, causing NaN pixel values in the HDF files, as well as black pixels in the JPG quicklooks:

AirMSPI_ER2_GRP_ELLIPSOID_20151204_174231Z_NorthPacificOcean-48N126W_SWPA_V006
AirMSPI_ER2_GRP_ELLIPSOID_20151204_174342Z_NorthPacificOcean-48N126W_SWPF_V006
AirMSPI_ER2_GRP_ELLIPSOID_20151204_174454Z_NorthPacificOcean-48N125W_SWPA_V006
AirMSPI_ER2_GRP_ELLIPSOID_20151204_174605Z_NorthPacificOcean-48N125W_SWPF_V006
AirMSPI_ER2_GRP_ELLIPSOID_20151204_174717Z_NorthPacificOcean-48N125W_SWPA_V006
AirMSPI_ER2_GRP_ELLIPSOID_20151204_174828Z_NorthPacificOcean-47N125W_SWPF_V006
AirMSPI_ER2_GRP_ELLIPSOID_20151204_175119Z_NorthPacificOcean-47N125W_SWPA_V006
AirMSPI_ER2_GRP_ELLIPSOID_20151204_175230Z_NorthPacificOcean-47N125W_SWPF_V006
AirMSPI_ER2_GRP_ELLIPSOID_20151204_175342Z_NorthPacificOcean-47N125W_SWPA_V006
AirMSPI_ER2_GRP_ELLIPSOID_20151204_175453Z_NorthPacificOcean-47N125W_SWPF_V006
AirMSPI_ER2_GRP_ELLIPSOID_20151204_175605Z_NorthPacificOcean-47N124W_SWPA_V006
AirMSPI_ER2_GRP_ELLIPSOID_20151204_175717Z_NorthPacificOcean-47N124W_SWPF_V006
AirMSPI_ER2_GRP_ELLIPSOID_20151204_181737Z_NorthPacificOcean-47N125W_SWPA_V006
AirMSPI_ER2_GRP_ELLIPSOID_20151204_181849Z_NorthPacificOcean-47N125W_SWPF_V006
AirMSPI_ER2_GRP_ELLIPSOID_20151204_182000Z_NorthPacificOcean-47N125W_SWPA_V006
AirMSPI_ER2_GRP_ELLIPSOID_20151204_182112Z_NorthPacificOcean-47N125W_SWPF_V006
AirMSPI_ER2_GRP_ELLIPSOID_20151204_182223Z_NorthPacificOcean-47N124W_SWPA_V006
AirMSPI_ER2_GRP_ELLIPSOID_20151204_182335Z_WA-OceanShores_SWPF_V006
AirMSPI_ER2_GRP_ELLIPSOID_20151204_183649Z_NorthPacificOcean-48N125W_SWPF_V006
AirMSPI_ER2_GRP_ELLIPSOID_20151204_183801Z_NorthPacificOcean-48N125W_SWPA_V006
AirMSPI_ER2_GRP_ELLIPSOID_20151204_183912Z_NorthPacificOcean-48N125W_SWPF_V006
AirMSPI_ER2_GRP_ELLIPSOID_20151204_185731Z_NorthPacificOcean-48N125W_SWPF_V006
AirMSPI_ER2_GRP_ELLIPSOID_20151204_185843Z_NorthPacificOcean-48N125W_SWPA_V006
AirMSPI_ER2_GRP_ELLIPSOID_20151204_185955Z_NorthPacificOcean-48N125W_SWPF_V006
AirMSPI_ER2_GRP_ELLIPSOID_20151204_190239Z_NorthPacificOcean-48N125W_SWPA_V006
AirMSPI_ER2_GRP_ELLIPSOID_20151204_190350Z_NorthPacificOcean-48N125W_SWPF_V006
AirMSPI_ER2_GRP_ELLIPSOID_20151204_190502Z_NorthPacificOcean-48N125W_SWPA_V006
AirMSPI_ER2_GRP_ELLIPSOID_20151204_190613Z_NorthPacificOcean-48N125W_SWPF_V006
AirMSPI_ER2_GRP_ELLIPSOID_20151204_190725Z_NorthPacificOcean-47N125W_SWPA_V006
AirMSPI_ER2_GRP_ELLIPSOID_20151204_190836Z_NorthPacificOcean-47N125W_SWPF_V006
AirMSPI_ER2_GRP_TERRAIN_20151204_175717Z_NorthPacificOcean-47N124W_SWPF_V006
AirMSPI_ER2_GRP_TERRAIN_20151204_182335Z_WA-OceanShores_SWPF_V006
AirMSPI_ER2_GRP_ELLIPSOID_20151213_202257Z_NorthPacificOcean-46N126W_SWPF_V006
AirMSPI_ER2_GRP_ELLIPSOID_20151213_202408Z_NorthPacificOcean-46N126W_SWPA_V006
AirMSPI_ER2_GRP_ELLIPSOID_20151213_202520Z_NorthPacificOcean-46N126W_SWPF_V006
AirMSPI_ER2_GRP_ELLIPSOID_20151213_203131Z_NorthPacificOcean-46N126W_SWPA_V006
AirMSPI_ER2_GRP_ELLIPSOID_20151213_203243Z_NorthPacificOcean-46N126W_SWPF_V006

Geolocation and band coregistration artifacts due to abrupt changes in the ER-2 attitude are observed in the following files:

AirMSPI_ER2_GRP_ELLIPSOID_20151110_182734Z_NorthPacificOcean-34N120W_SWPA_V006
AirMSPI_ER2_GRP_ELLIPSOID_20151110_182843Z_NorthPacificOcean-34N120W_SWPF_V006
AirMSPI_ER2_GRP_ELLIPSOID_20151110_183208Z_NorthPacificOcean-34N120W_SWPA_V006
AirMSPI_ER2_GRP_ELLIPSOID_20151110_183317Z_NorthPacificOcean-34N120W_SWPF_V006
AirMSPI_ER2_GRP_TERRAIN_20151110_183317Z_NorthPacificOcean-34N120W_SWPF_V006
AirMSPI_ER2_GRP_ELLIPSOID_20151124_181609Z_NorthPacificOcean-47N127W_SWPF_V006
AirMSPI_ER2_GRP_ELLIPSOID_20151210_190246Z_NorthPacificOcean-47N126W_SWPA_V006
AirMSPI_ER2_GRP_ELLIPSOID_20151213_165854Z_NorthPacificOcean-48N126W_SWPF_V006

The flights on November 24 and December 4 took off before sunrise. AirMSPI imagery acquired early during the day may be dimmer and noisier than usual.

7 REFERENCES

Diner, D.J., A. Davis, B. Hancock, G. Gutt, R.A. Chipman, and B. Cairns (2007). Dual photoelastic modulator-based polarimetric imaging concept for aerosol remote sensing. *Appl. Opt.* **46**, 8428-8445.

Diner, D.J., A. Davis, B. Hancock, S. Geier, B. Rheingans, V. Jovanovic, M. Bull, D.M. Rider, R.A. Chipman, A. Mahler, and S.C. McClain (2010). First results from a dual photoelastic modulator-based polarimetric camera. *Appl. Opt.* **49**, 2929-2946.

Diner, D.J., F. Xu, J.V. Martonchik, B.E. Rheingans, S. Geier, V.M. Jovanovic, A. Davis, R.A. Chipman, and S.C. and McClain (2012). Exploration of a polarized surface bidirectional reflectance model using the Ground-based Multiangle SpectroPolarimetric Imager. *Atmosphere* **3**, 591-619.

Diner, D.J., F. Xu, M.J. Garay, J.V. Martonchik, B.E. Rheingans, S. Geier, A. Davis, B.R. Hancock, V.M. Jovanovic, M.A. Bull, K. Capraro, R.A. Chipman, and S.C. McClain (2013a). The Airborne Multiangle SpectroPolarimetric Imager (AirMSPI): a new tool for aerosol and cloud remote sensing. *Atmos. Meas. Tech*. **6**, 2007-2025.

Diner, D.J., M.J. Garay, O.V. Kalashnikova, B.E. Rheingans, S. Geier, M.A. Bull, V.M. Jovanovic, F. Xu, C.J. Bruegge, A. Davis, K. Crabtree, and R.A. Chipman (2013b). Airborne Multiangle SpectroPolarmetric Imager (AirMSPI) observations over California during NASA's Polarimeter Definition Experiment (PODEX). *SPIE Proc*. **8873**, 88730B-2.

Jovanovic, V.M., M. Bull, D.J. Diner, S. Geier, and B. Rheingans (2012). Automated data production for a novel Airborne Multiangle SpectroPolarimetric Imager (AirMSPI). *Int. Arch. Photogramm. Remote Sens. Spatial Inf. Sci.*, **XXXIX-B1**, 33-38.

Mahler, A., D.J. Diner, and R.A. Chipman (2011). Analysis of static and time-varying polarization errors in the multiangle spectropolarimetric imager. *Appl. Opt.* **50**, 2080-2087.

Palmer, J.M. (1984). Effective bandwidths for LANDSAT-4 and LANDSAT-D' Multispectral Scanner and Thematic Mapper subsystems. *IEEE Trans. Geosci. Rem. Sens.* **GE-22**, 336-338.

Van Harten, G., Diner, D. J., Daugherty, B. J. S., Rheingans, B. E., Bull, M. A., Seidel, F. C., Chipman, R. A., Cairns, B., Wasilewski, A. P., and Knobelspiesse, K. (2018). Calibration and validation of Airborne Multiangle SpectroPolarimetric Imager (AirMSPI) polarization measurements. Applied Optics (in press).

Wehrli, C. (1985). "Extraterrestrial Solar Spectrum", Publication no. 615, Physikalisch Meteorologisches Observatorium + World Radiation Center (PMO/WRC) Davos Dorf, Switzerland, July 1985.

8 APPENDIX

Acronym List:

AirMSPI	Airborne Multiangle SpectroPolarimetric Imager
AMPR	Advanced Microwave Precipitation Radiometer
AOLP	Angle of Linear Polarization
ASD	Analytical Spectral Devices
ASDC	Atmospheric Science Data Center
AU	Astronomical Unit
CPL	Cloud Physics Lidar
CRS	Cloud Radar System
DEM	Digital Elevation Model
DN	Digital Number
DOLP	Degree of Linear Polarization
eMAS	Enhanced MODIS Airborne Simulator
EOS	Earth Observing System
EXRAD	ER-2 X-band Doppler Radar
GCP	Ground Control Point
HDF-EOS	Hierarchical Data Format for EOS
HIWRAP	High-altitude Imaging Wind and Rain Airborne Profiler
JPL	Jet Propulsion Laboratory
LaRC	Langley Research Center (NASA)
LED	Light-emitting diode
MISR	Multi-angle Imaging SpectroRadiometer
NASA	National Aeronautics and Space Administration
NED	National Elevation Dataset
NIST	National Institute of Standards and Technology
PEM	Photoelastic modulator
RADEX	Radar Definition Experiment
RDQI	Radiometric Data Quality Indicator
SCF	Science Computing Facility
SDP	Science Data Processing
SPEX-PR	SPEX engineering flights + Porter Ranch gas leak overflights
SI	*Système international*
SRF	Spectral Response Function
USGS	United States Geological Survey

UTM	Universal Transverse Mercator
UV	Ultraviolet
WGS84	World Geodetic System 1984